EPJ Web of Conferences **163**, 00021 (2017) DOI: 10.1051/epjconf/201716300021
FUSION17

Skyrme tensor force in the collision ^{16}O+^{40}Ca

Lu Guo[1,⋆], *Chong* Yu[1], *Long* Shi[1], and *Cédric* Simenel[2]

[1] *School of Physics, University of Chinese Academy of Sciences, Beijing 100049, China*
[2] *Department of Nuclear Physics, RSPE, Australian National University, Canberra, Australia*

Abstract. The role of tensor force is investigated by using the time-dependent Hartree-Fock (TDHF) theory in the collision ^{16}O+^{40}Ca. The full tensor force is incorporated in our TDHF implementation. The calculations are performed in three-dimensional Cartesian coordinate without any symmetry restrictions. We study the effect of tensor force on Coulomb barrier, upper fusion threshold energy, and energy contribution of the time-odd and tensor terms in Skyrme energy functional. The Coulomb barrier obtained from the energy functional with frozen density approximation is compared with the available experimental data. We find that the tensor force may change the upper fusion threshold energy in the order of a few MeV for the collision ^{16}O+^{40}Ca. The tensor force has a non-negligible effect in heavy-ion collisions.

1 Introduction

The microscopic description of heavy-ion collisions such as time-dependent Hartree-Fock (TDHF) theory provides a useful foundation for a fully microscopic many-body theory. The dynamical and quantum effects have been automatically taken into account in TDHF theory. It has wide applications in fusion [1–10], fission [11–16], transfer reaction [17–21], deep inelastic collisions [22–28], quasi-fission [21, 29–33], and giant resonances [34–41]. For a review, see Refs. [42, 43].

TDHF theory was proposed by Dirac in 1930 [44] and was first applied in nuclear physics in 1976 [45]. After the first application, many groups in the late 70s and 80s performed more extensive calculations in nuclear large amplitude collective motion [46]. However, at that time, limited computer capacity restricted most calculations with many approximations. For instance, the reaction was assumed to be in an axial symmetric plane and a simplified Skyrme force with the omission of spin-orbit coupling was used. These approximations turned out to be a hindrance for the theoretical development. For example, TDHF calculations predicted that for ^{16}O+^{16}O reaction at $E_{\rm c.m.}$ = 34 MeV the partial waves $L \leq 6$ do not lead to fusion and the corresponding deep inelastic cross section was expected to be 132 mb [47]. According to TDHF prediction, an experiment to search for a fusion L window was carried out. However, experimentally there is no evidence for the occurrence of such phenomenon predicted by TDHF calculations [47]. This conflict between TDHF prediction and experimental observations is called the puzzle of small fusion window, and promotes the theoretical development.

A few years later in 1986, Umar *et. al* included the time-even terms of spin-orbit force in TDHF calculations [48], and found the upper fusion threshold energy was increased by more than two times. This indicates that earlier TDHF calculations without spin-orbit coupling underestimated the energy dissipation from the collective kinetic energy into the internal excitations so that the energy window of fusion reactions was too small in comparison with the experiments. After including the spin-orbit coupling, more intrinsic degrees of freedom is accessable and the dissipation is enhanced. The inclusion of time-even spin-orbit force in TDHF solved the puzzle of small fusion window. However, a meaningful collision theory should satisfy Galilean invariance which guarantees the calculation results will not depend on the choice of the frame of reference. This invariance is particularly important for reaction dynamics so that both the time-even and time-odd terms of spin-orbit force should be included simultaneously. In recent years, TDHF calculations with the full spin-orbit force become possible thanks to the development of computational power. The strong spin-excitation was shown in spin-saturated system ^{16}O+^{16}O [22]. The full spin-orbit force was found to contribute about 40%∼65% of the total dissipation depending on the different Skyrme parameters and bombarding energies [26].

These studies indicate the nucleon-nucleon interaction plays a significant role in heavy-ion collisions. The most obviously missing component of nuclear force is tensor force, which is well known to be crucial to explain the properties of the deuteron. In nuclear structure, the tensor force plays an important role in the shell evolution of exotic nuclei [49], spin-orbit splitting [50, 51], deformation [52], rotation [53], Gamow-Teller and spin-dipole excitations [54]. However, in heavy-ion collisions the full tensor force has been neglected in most calculations due to the complexity of collision dynamics. In Ref. [55], the

⋆e-mail: luguo@ucas.ac.cn

© The Authors, published by EDP Sciences. This is an open access article distributed under the terms of the Creative Commons Attribution License 4.0 (http://creativecommons.org/licenses/by/4.0/).

time-even spin-current tensor was shown to become important as the increase of the mass of colliding systems. The role of time-even tensor force in the dissipation dynamics in deep-inelastic collisions has been explored in Ref. [26]. Recently the full tensor force was shown to play a non-negligible effect in ^{16}O+^{16}O inelastic collisions [9, 28].

The article is organized as follows. Section 2 will present the TDHF theory with the full version of Skyrme interaction and energy density functional including the tensor force. In Sec. 3 we illustrate the role of tensor force in the asymmetric reaction ^{16}O+^{40}Ca. A summary is given in Sec. 4.

2 Theoretical method

Starting from the time-dependent action

$$S = \int_{t_1}^{t_2} dt \langle \Psi(\mathbf{r},t)|H - i\hbar\partial_t|\Psi(\mathbf{r},t)\rangle, \tag{1}$$

and applying the variational principal $\delta S = 0$ with respect to the many-body wave-function $\Psi(\mathbf{r},t)$, one may obtain the time evolution of mean-field

$$i\hbar\partial_t\phi_\lambda = \hat{h}\phi_\lambda. \tag{2}$$

In the above TDHF equation, the many-body wave-function has been approximated as the Slater determinant composed by the single-particle states ϕ_λ

$$\Psi(\mathbf{r},t) = \frac{1}{\sqrt{N!}}\det\{\phi_\lambda(\mathbf{r},t)\}. \tag{3}$$

The initial wave-functions in dynamical evolution employ the nuclear ground state obtained from HF equation

$$\hat{h}\varphi_\lambda(\mathbf{r}) = \epsilon_\lambda\varphi_\lambda(\mathbf{r}). \tag{4}$$

The time evolution of single-particle states is expressed as

$$\phi_\lambda(\mathbf{r}, t+\Delta t) = e^{-i\hat{h}\Delta t/\hbar}\phi_\lambda(\mathbf{r},t), \tag{5}$$

with $\hat{h}$ the single-particle Hamiltonian. Here $\mathbf{r}$ denotes the three-dimensional Cartesian coordinate and the spin of nucleon.

We employ the Skyrme effective interaction in our TDHF calculation

$$\begin{aligned}
v(\mathbf{r}_1,\mathbf{r}_2) &= t_0(1+x_0\hat{P}_\sigma)\delta(\mathbf{r}_1-\mathbf{r}_2) \\
&+ \frac{1}{2}t_1(1+x_1\hat{P}_\sigma)[\mathbf{k}'^2\delta(\mathbf{r}_1-\mathbf{r}_2)+\delta(\mathbf{r}_1-\mathbf{r}_2)\mathbf{k}^2] \\
&+ t_2(1+x_2\hat{P}_\sigma)\mathbf{k}'\delta(\mathbf{r}_1-\mathbf{r}_2)\mathbf{k} \\
&+ \frac{1}{6}t_3(1+x_3\hat{P}_\sigma)\rho^\alpha(\frac{\mathbf{r}_1+\mathbf{r}_2}{2})\delta(\mathbf{r}_1-\mathbf{r}_2) \\
&+ iW_0(\sigma_1+\sigma_2)\cdot\mathbf{k}'\times\delta(\mathbf{r}_1-\mathbf{r}_2)\mathbf{k} \\
&+ \frac{t_e}{2}\Big\{[3(\sigma_1\cdot\mathbf{k}')(\sigma_2\cdot\mathbf{k}')-(\sigma_1\cdot\sigma_2)\mathbf{k}'^2]\delta(\mathbf{r}_1-\mathbf{r}_2) \\
&+ \delta(\mathbf{r}_1-\mathbf{r}_2)[3(\sigma_1\cdot\mathbf{k})(\sigma_2\cdot\mathbf{k})-(\sigma_1\cdot\sigma_2)\mathbf{k}^2]\Big\} \\
&+ t_o\Big\{3(\sigma_1\cdot\mathbf{k}')\delta(\mathbf{r}_1-\mathbf{r}_2)(\sigma_2\cdot\mathbf{k})-(\sigma_1\cdot\sigma_2)\mathbf{k}' \\
&\delta(\mathbf{r}_1-\mathbf{r}_2)\mathbf{k}\Big\},
\end{aligned} \tag{6}$$

where t_i, x_j ($i, j = 0, ..., 3$), W_0, α, t_e, and t_o are the Skyrme parameters. In the above equation, from the sixth to ninth line represents the tensor force, in which the coupling constants t_e and t_o denote the strength of the triplet-even and triplet-odd tensor interactions, respectively. The operator $\mathbf{k} = \frac{1}{2i}(\nabla_1 - \nabla_2)$ acts on the right , $\mathbf{k}' = -\frac{1}{2i}(\nabla'_1 - \nabla'_2)$ acts on the left. The spin exchange operator is $P_\sigma = \frac{1}{2}(1+\sigma_1\sigma_2)$.

It is natural to express the Skyrme interaction with the energy density functional (EDF)

$$E = \int d^3r\mathcal{H}(\rho,\tau,\mathbf{j},\mathbf{s},\mathbf{T},\mathbf{J};\mathbf{r}). \tag{7}$$

In above equation, the number density ρ, kinetic density τ, current density $\mathbf{j}$, spin density $\mathbf{s}$, spin-kinetic density $\mathbf{T}$, and spin-current pseudotensor density $\mathbf{J}$ are defined as

$$\begin{aligned}
\rho_q(\mathbf{r}) &= \rho_q(\mathbf{r},\mathbf{r}')|_{\mathbf{r}=\mathbf{r}'} = \sum_\sigma \rho_q(\mathbf{r}\sigma,\mathbf{r}'\sigma'), \\
s_q(\mathbf{r}) &= s_q(\mathbf{r},\mathbf{r}')|_{\mathbf{r}=\mathbf{r}'} = \sum_{\sigma\sigma'} \rho_q(\mathbf{r}\sigma,\mathbf{r}'\sigma')\langle\sigma'|\hat{\sigma}|\sigma\rangle, \\
\tau_q(\mathbf{r}) &= \nabla\cdot\nabla'\rho_q(\mathbf{r},\mathbf{r}')|_{\mathbf{r}=\mathbf{r}'}, \\
j_q(\mathbf{r}) &= -\frac{i}{2}(\nabla-\nabla')\rho_q(\mathbf{r},\mathbf{r}')|_{\mathbf{r}=\mathbf{r}'}, \\
J_{q,\mu\nu}(\mathbf{r}) &= -\frac{i}{2}(\nabla_\mu-\nabla'_\mu)s_{q,\nu}(\mathbf{r},\mathbf{r}')|_{\mathbf{r}=\mathbf{r}'}, \\
T_{q,\mu}(\mathbf{r}) &= \nabla\cdot\nabla' s_{q,\mu}(\mathbf{r},\mathbf{r}')|_{\mathbf{r}=\mathbf{r}'}, \\
F_{q,\mu}(\mathbf{r}) &= \frac{1}{2}\sum_{\nu=x}^{z}(\nabla_\mu\nabla'_\nu+\nabla'_\mu\nabla_\nu)s_\nu(\mathbf{r},\mathbf{r}')|_{\mathbf{r}=\mathbf{r}'}.
\end{aligned} \tag{8}$$

Here, $q = n(p)$ stands for neutron (proton).

From these densities, one can define the isoscalar ($t = 0$) and isovector ($t = 1$) densities and currents as

$$\begin{aligned}
\rho_0(\mathbf{r}) &= \rho_n(\mathbf{r}) + \rho_p(\mathbf{r}), \\
\rho_1(\mathbf{r}) &= \rho_n(\mathbf{r}) - \rho_p(\mathbf{r}).
\end{aligned} \tag{9}$$

With the above definitions, the full version of Skyrme energy functional is expressed as

$$\begin{aligned}
\mathcal{H} = \mathcal{H}_0 + \sum_{t=0,1}\Big\{ & A_t^s\mathbf{s}_t^2 + \Big(A_t^{\Delta s}+B_t^{\Delta s}\Big)\mathbf{s}_t\cdot\Delta\mathbf{s}_t + B_t^{\nabla s}(\nabla\cdot\mathbf{s}_t)^2 \\
& + (A_t^T+B_t^T)\Big(\mathbf{s}_t\cdot\mathbf{T}_t - \sum_{\mu,\nu=x}^{z}J_{t,\mu\nu}J_{t,\mu\nu}\Big) \\
& + B_t^F\Big[\mathbf{s}_t\cdot\mathbf{F}_t - \frac{1}{2}\Big(\sum_{\mu=x}^{z}J_{t,\mu\mu}\Big)^2 - \frac{1}{2}\sum_{\mu,\nu=x}^{z}J_{t,\mu\nu}J_{t,\nu\mu}\Big]\Big\},
\end{aligned} \tag{10}$$

where $\mathcal{H}_0$ is the basic Skyrme functional used in Sky3D code [56] and most TDHF calculations. In our code, we incorporated the full version of Skyrme energy functional as shown in Eq. (10), including all the terms from central, spin-orbit and tensor forces. These new terms have been clarified to be especially important in the studies of nuclear structure. The basic functional $\mathcal{H}_0$ used in Sky3D

code [56] is expressed as

$$\mathcal{H}_0 = \sum_{t=0,1} \Big\{ A_t^{\rho}\rho_t^2 + A_t^{\Delta\rho}\rho_t\Delta\rho_t + A_t^{\tau}\Big(\rho_t\tau_t - \mathbf{j}_t^2\Big) + A_t^{\nabla J}\rho_t\nabla\cdot\mathbf{J}_t + A_t^{\nabla J}\mathbf{s}_t\cdot\nabla\times\mathbf{j}_t\Big\}. \quad (11)$$

The coupling constants A and B appearing in Eqs. (10) and (11) have been defined in Refs. [51, 57]. Some authors used the coupling constants C which is the sum of parameters A and B, $C = A + B$. The terms with the coupling constants A come from the Skyrme central and spin-orbit forces, while those with the B parameters are from the tensor force. In the calculations, we set $C_t^{\nabla S} = C^{\Delta S} = 0$ because the terms containing the gradient of spin-density may cause the spin instability both in nuclear structure and reaction studies as pointed out in Refs. [28, 51].

In the energy functional Eq. (10), the spin-current pseudotensor density $\mathbf{J}$ is expressed in its Cartesian components $J_{\mu\nu}$. In Ref. [58] the spin-current density has been decomposed into pseudoscalar, (antisymmetric) vector, and (symmetric) traceless pseudotensor components as

$$J_{\mu\nu}(r) = \frac{1}{3}\delta_{\mu\nu}J^{(0)}(r) + \frac{1}{2}\sum_{k=x}^{z}\varepsilon_{\mu\nu k}J_k^{(1)}(r) + J_{\mu\nu}^{(2)}(r). \quad (12)$$

Here $\delta_{\mu\nu}$ is the Kronecker symbol and $\varepsilon_{\mu\nu k}$ is the Levi-Civita tensor. The pseudoscalar $J^{(0)}$, vector $J^{(1)}$, and pseudotensor $J^{(2)}$ components are given in terms of the Cartesian form

$$\begin{aligned} J^{(0)}(\mathrm{r}) &= \sum_{\mu=x}^{z} J_{\mu\mu}(\mathrm{r}), \\ J_k^{(1)}(\mathrm{r}) &= \sum_{\mu\nu=x}^{z} \varepsilon_{k\mu\nu}J_{\mu\nu}(\mathrm{r}), \\ J_{\mu\nu}^{(2)}(\mathrm{r}) &= \frac{1}{2}[J_{\mu\nu}(r) + J_{\nu\mu}(\mathrm{r})] - \frac{1}{3}\delta_{\mu\nu}\sum_{\mathrm{k=x}}^{\mathrm{z}}\mathrm{J_{kk}(r)}. \end{aligned} \quad (13)$$

The vector spin-current density $J^{(1)}(\mathbf{r}) \equiv \mathbf{J}(\mathbf{r})$ is often called spin-orbit current, as it enters the spin-orbit functional in Eq. (11). The terms of energy functional involving the spin-current density in Eq. (10) can be instead expressed as

$$\sum_{\mu,\nu=x}^{z} J_{\mathrm{t},\mu\nu}J_{\mathrm{t},\mu\nu} = \frac{1}{3}J_t^{(0)2} + \frac{1}{2}J_t{}^2 + \sum_{\mu,\nu=x}^{z} J_{\mathrm{t},\mu\nu}^{(2)}J_{\mathrm{t},\mu\nu}^{(2)}, \quad (14)$$

$$\frac{1}{2}\Big(\sum_{\mu=x}^{z} J_{\mathrm{t},\mu\mu}\Big)^2 + \frac{1}{2}\sum_{\mu,\nu=x}^{z} J_{\mathrm{t},\mu\nu}J_{\mathrm{t},\nu\mu} = \frac{2}{3}J_t^{(0)2} - \frac{1}{4}J_t{}^2 + \frac{1}{2}\sum_{\mu,\nu=x}^{z} J_{\mathrm{t},\mu\nu}^{(2)}J_{\mathrm{t},\mu\nu}^{(2)}. \quad (15)$$

To test the accuracy of numerical calculations, the energy functional involving the spin-current density has been implemented by using the above two approaches in our code.

Table 1. Isoscalar and isovector tensor coupling constants $C_0^J = A_0^J + B_0^J$ and $C_1^J = A_1^J + B_1^J$ (in MeV·fm^5) for the five sets of Skyrme parametrizations.

Force	C_0^J	C_1^J
SLy5	0.0	60.0
SLy5t	-20.0	-65.0
T22	0.0	0.0
T26	120.0	120.0
T44	120.0	0.0

In the next section, we will show the energy contributions with this two approaches are identical, as they should be.

The set of nonlinear TDHF equations has been solved on a three-dimensional Cartesian coordinate and without any symmetry restrictions. We calculate the ground state of ^{16}O and ^{40}Ca in a numerical box of $24\times24\times24$ fm^3. For the dynamical evolution of reaction ^{16}O+^{40}Ca, we used a box with $32\times24\times32$ fm^3 grid points and grid spacing 1.0 fm. The initial distance between the projectile and target is taken to be 20 fm. From infinity to initial distance the nucleus was assumed to move on a pure Rutherford trajectory so that the initial boost are properly treated in TDHF evolution. We expand the Taylor expansion up to the sixth order and employ a time step $\Delta t = 0.2$ fm/c in the dynamical evolution. The choice of these parameters guarantees a good numerical accuracy during the dynamical evolution for all the cases studied here. The total TDHF energy and particle number have been well conserved and shifted less than 0.1 MeV and 0.01, respectively.

3 Results and discussions

We employ the full version of Skyrme energy functional as shown in Eq. (10) in our calculations. The static properties and reaction dynamics are treated with the same energy density functional and a unified theoretical framework. To examine the accuracy of our code, we compared our results with those obtained by other code in three aspects. First, we have reproduced the upper fusion threshold energy in the collision ^{16}O+^{16}O reported in Ref. [28] within the accuracy of 1 MeV by our code. Second, we calculated the energy contribution from the new terms as a function of time, and our results reproduced those reported in Ref. [28] within a negligible discrepancy. Third, we implemented the energy functional involving the spin-current density in two approaches as shown in Eqs. (14) and (15) in our code, and found that the results with two approaches are identical as they should be and also reproduced those shown in Ref. [28].

In present work, we employ the five sets of Skyrme parametrizations SLy5 [60, 61], SLy5t [50], and T22,T26 and T44 [51] to study the effect of tensor force in the collision dynamics of ^{16}O+^{40}Ca reaction. The isoscalar and isovector tensor coupling constants $C_0^J = A_0^J + B_0^J$ and $C_1^J = A_1^J + B_1^J$ are shown in Tab. 1 for this five sets parameters with a wide range of coupling constants. Note that the parameters of Skyrme tensor force have been fitted in two ways. One is to fit the parameters of tensor force based

Table 2. Energy (in MeV) and radii (in fm) of the Coulomb barrier obtained with the frozen density approximation for the five sets of Skyrme parametrizations and experimental data [59] in the collisions ^{16}O+^{40}Ca.

Force	V(MeV)	R(fm)
SLy5	23.36	9.20
SLy5t	23.36	9.20
T22	23.34	9.21
T26	23.33	9.21
T44	23.21	9.25
Expt.	23.06	9.21

Table 3. Upper fusion threshold energies (in MeV) for the five sets of Skyrme parametrizations in the collisions ^{16}O+^{40}Ca.

Force	Threshold (MeV)
SLy5	142
SLy5t	145
T22	138
T26	143
T44	140

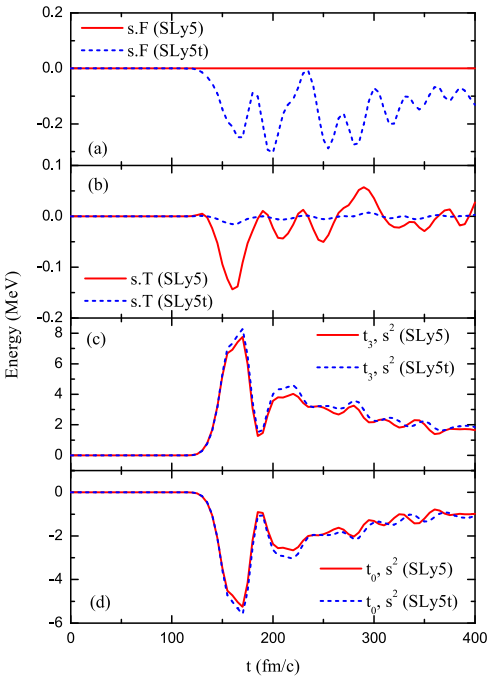

Figure 1. Energy contributions from the terms involving time-odd densities and currents for head-on collisions ^{16}O+^{40}Ca with SLy5 and SLy5t parametrizations at $E_{\rm c.m.}$ = 170 MeV.

on the existing Skyrme force, e.g., SLy5 plus tensor force denoted as SLy5t. The other is to fit all the Skyrme parameters on the same footing, e.g., the set of T*IJ* parametrizations with a wide range of isoscalar and isovector tensor couplings. With such fitting procedure, one may draw a different physical scenario. The effect of pure tensor force can be clarified by comparing the results with SLy5 and SLy5t. For the T*IJ* parametrizations, the calculations can figure out the role of isoscalar and isovector tensor terms in collision dynamics.

The energy and radii of Coulomb barrier are listed in Tab. 2 for ^{16}O+^{40}Ca with the five sets of forces and the experimental data [59]. Here the Coulomb barrier is obtained by the frozen density (FD) approximation within the EDF theory [62–64]. The interaction potential in the approaching phase can be expressed as

$$V^{\rm FD}(R) = E[\rho_{\rm P+T}](R) - E[\rho_{\rm T}] - E[\rho_{\rm P}]. \qquad (16)$$

$\rho_{\rm P+T} = \rho_{\rm P} + \rho_{\rm T}$ is the sum of ground state density of projectile and target at the relative distance R, and $E[\rho_{\rm P+T}](R)$ is the Skyrme EDF as shown in Eq (10). Note that the Pauli principle and the coupling between the collective motion and intrinsic states have been neglected in FD approximation. When the overlap of two densities is small, e.g., at the position of Coulomb barrier, EDF with FD approximation is a good tool to estimate the Coulomb barrier. However, at the smaller relative distance, since the Pauli effect is strong, FD approximation will not properly account for the interaction potential [65].

The energy and radii of Coulomb barrier with SLy5t are observed to be exactly same as those with SLy5 for ^{16}O+^{40}Ca, as expected, because the tensor force has no contribution to the ground state EDF for the spin-saturated nuclei ^{16}O and ^{40}Ca. There exist some differences among the T22,T26 and T44 parameter sets. These differences, for the spin-saturated system, come from the rearrangement of other terms of Skyrme EDF in the fit of the parametrizations. Note that the structure of ^{16}O and ^{40}Ca, for instance, matter and charge radii, has small difference for T22,T26 and T44 parameters, which may cause a slight change of the barrier height. The Coulomb barrier with FD-EDF overestimates the experimental data due to its omission of the coupling between the collective motion and single particle degrees of freedom [66].

The upper fusion threshold is quite sensitive to the details of Skyrme EDF as reported in Ref. [3]. The inclusion of pure tensor force SLy5t increased the upper threshold by 3 MeV. The SLy5 and T22 have the same isoscalar coupling constants, and the upper fusion threshold is found to reduce as the decrease of isovector coupling. The same trend is also observed for T26 and T44. By comparing T22 and T44 with the same isovector coupling, the increase of isoscalar coupling increases the upper fusion threshold. Our results in ^{16}O+^{40}Ca are consistent with the findings in Ref. [28] for ^{16}O+^{16}O.

The energy contributions from the terms involving time-odd densities and currents (a) $s \cdot F$, (b) $s \cdot T$, (c) s^2 with t_0 parameter, and (d) s^2 with t_3 parameter are examined for ^{16}O+^{40}Ca head-on collisions with SLy5 and SLy5t parametrizations at $E_{\rm c.m.}$ = 170 MeV. The results are shown in Fig. 1. This is deep-inelastic collisions as seen from Tab. 3. These terms were not included in Sky3D code [56]. At the initial time, the energy contribution from these terms both for SLy5 and SLy5t are zero, as expected, because these time-odd terms contribute zero for the ground state of even-even nuclei. Since the term $s \cdot F$ comes from the pure tensor force, its energy with SLy5 remains zero during the time evolution. For SLy5t because

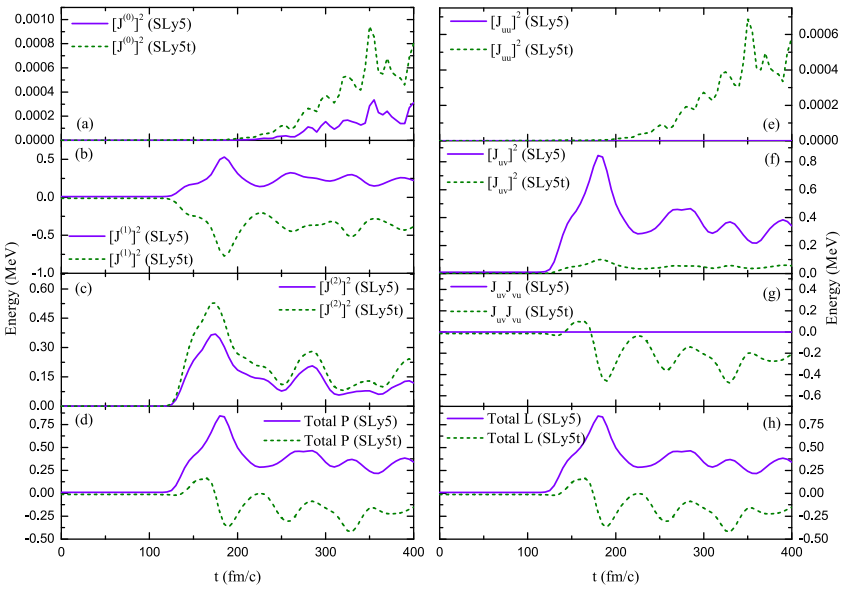

Figure 2. The energy contribution from the time-even terms in head-on collisions ^{16}O+^{40}Ca at $E_{\mathrm{c.m.}}$ = 170 MeV.

the inclusion of tensor force changes the time-dependent mean-field and hence the densities s and F itself, the energy contribution keeps to be zero in the early stage and then starts to oscillate. Since $s \cdot T$ term comes from both the central and tensor forces, its energy with SLy5 evolves with time, while for SLy5t the more pronounced effect appears compared with SLy5. The s^2 terms from the central force are found to have similar trends.

In order to test the numerical realization of our code and understand the contribution of tensor force in energy functional, we calculate the energy contribution from the J^2 terms both in its coupled form and Cartesian form as given in Eqs. (14) and (15). The left column in Fig. 2(a-d) shows the energy contribution of scalar, vector, and tensor components of J^2, and the summation of these three terms, while the right column in Fig. 2(e-h) is the contribution from the diagonal, symetric and anti-symetric components and also the corresponding summation. The total contribution calculated with two approaches are exactly identical shown in Fig. 2(d) and (h), as they should be.

We also check the final kinetic energy of the fragments for the case of $E_{\mathrm{c.m.}}$=170 MeV, which is 28.1 MeV and 26.3 MeV for SLy5 and SLy5t, respectively. This energy provides the amount of energy transferred from relative motion to internal degrees of freedom, and could be a direct measure of the energy dissipation.

The contribution to the total energy from J^2 term is shown in Fig. 3 for the five sets of Skyrme parameters in the collisions ^{16}O+^{40}Ca at $E_{\mathrm{c.m.}}$ = 46.5 MeV and b = 5.0 fm. In the early stage of dynamical evolution, the energy from J^2 keeps constant as that in the ground state. As time evolves, these terms are highly excited in the dynamic process and present an evident effect in heavy-ion collisions of spin-saturated system ^{16}O+^{40}Ca , while they have negligible effect in the ground state of spin-saturated nucleus. The perturbative addition of tensor terms with SLy5t has an opposite sign with respect to the other four forces. The TIJ forces contribute to the energy up to a few MeV.

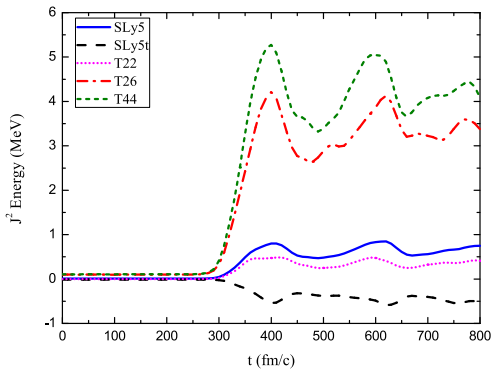

Figure 3. The energy contribution from the J^2 terms in the collisions ^{16}O+^{40}Ca at $E_{\mathrm{c.m.}}$ = 46.5 MeV and b = 5.0 fm.

4 Conclusion

We study the role of tensor force within the TDHF theory for the collision ^{16}O+^{40}Ca. The full tensor force is incorporated in our TDHF implementation. The calculations are carried out in three-dimensional and symmetry unrestricted Cartesian coordinate. We employ the five sets of Skyrme parametrizations SLy5, SLy5t, T22, T26 and T44 with a wide range of isoscalar and isovector tensor coupling to study the role of tensor force in heavy-ion collision dynamics. The tensor force is found to change the upper fusion threshold energy in the order of a few MeV in the spin-saturated system ^{16}O+^{40}Ca. The time-odd and tensor terms in Skyrme energy functional show an evident effect in the dynamical evolution. The tensor force plays a non-negligible effect in heavy-ion collisions.

5 Acknowledgments

This work is partly supported by the Natural Science Foundation of China under Grants Nos. 11175252 and 11575189, President Fund of UCAS, the NSFC-JSPS international cooperation program under Grant No. 11711540016, and the Australian Research Council Grants Nos. FT120100760 and DP160101254. The computation of this work was performed in the Tianhe-1A supercomputer located in the Chinese National Supercomputer Center.

References

[1] C. Simenel *et al.*, Phys. Rev. Lett. **86**, 2971 (2001)
[2] C. Simene *et al.*, Phys. Rev. Lett. **93**, 102701 (2004)
[3] A.S. Umar, V.E. Oberacker, Phys. Rev. C **73**, 054607 (2006)
[4] K. Washiyama, D. Lacroix, Phys. Rev. C **78**, 024610 (2008)
[5] L. Guo, T. Nakatsukasa, EPJ WEB of CONFERENCE **38**, 09003 (2012)
[6] C. Simenel *et al.*, Phys. Rev. C **88**, 024617 (2013)
[7] K. Washiyama, Phys. Rev. C **91**, 064607 (2015)
[8] M. Tohyama, A.S. Umar, Phys. Rev. C **93**, 034607 (2016)
[9] G.L. SHI Long, Nuclear Physics Review **34**, 41 (4) (2017)
[10] K. Godbey *et al.*, Phys. Rev. C **95**, 011601(R) (2017)
[11] C. Simenel, A.S. Umar, Phys. Rev. C **89**, 031601 (2014)
[12] G. Scamps *et al.*, Phys. Rev. C **92**, 011602 (2015)
[13] P. Goddard *et al.*, Phys. Rev. C **92**, 054610 (2015)
[14] P.M. Goddard *et al.*, Phys. Rev. C **93**, 014620 (2016)
[15] A. Bulgac *et al.*, Phys. Rev. Lett. **116**, 122504 (2016)
[16] Y. Tanimura *et al.*, Phys. Rev. Lett. **118**, 152501 (2017)
[17] C. Simenel, Phys. Rev. Lett. **105**, 192701 (2010)
[18] G. Scamps, D. Lacroix, Phys. Rev. C **87**, 014605 (2013)
[19] K. Sekizawa, K. Yabana, Phys. Rev. C **88**, 014614 (2013)
[20] N. Wang, L. Guo, Physics Letters B **760**, 236 (2016)
[21] K. Sekizawa, K. Yabana, Phys. Rev. C **93**, 054616 (2016)
[22] J.A. Maruhn *et al.*, Phys. Rev. C **74**, 027601 (2006)
[23] L. Guo *et al.*, Phys. Rev. C **76**, 014601 (2007)
[24] L. Guo *et al.*, Phys. Rev. C **77**, 041301(R) (2008)
[25] C. Simenel, Phys. Rev. Lett. **106**, 112502 (2011)
[26] G.F. Dai *et al.*, Phys. Rev. C **90**, 044609 (2014)
[27] G.F. Dai *et al.*, Sci. China-Phys. Mech. Astron. **57**, 1618 (2014)
[28] P.D. Stevenson *et al.*, Phys. Rev. C **93**, 054617 (2016)
[29] C. Golabek, C. Simenel, Phys. Rev. Lett. **103**, 042701 (2009)
[30] A. Wakhle *et al.*, Phys. Rev. Lett. **113**, 182502 (2014)
[31] V.E. Oberacker *et al.*, Phys. Rev. C **90**, 054605 (2014)
[32] A.S. Umar *et al.*, Phys. Rev. C **92**, 024621 (2015)
[33] A.S. Umar *et al.*, Phys. Rev. C **94**, 024605 (2016)
[34] C. Simenel, P. Chomaz, Phys. Rev. C **68**, 024302 (2003)
[35] J.A. Maruhn *et al.*, Phys. Rev. C **71**, 064328 (2005)
[36] T. Nakatsukasa, K. Yabana, Phys. Rev. C **71**, 024301 (2005)
[37] A.S. Umar, V.E. Oberacker, Phys. Rev. C **71**, 034314 (2005)
[38] P.G. Reinhard *et al.*, Eur. Phys. J. A **32**, 19 (2007)
[39] C. Simenel, P. Chomaz, Phys. Rev. C **80**, 064309 (2009)
[40] B. Avez, C. Simenel, Eur. Phys. J. A **49**, 76 (2013)
[41] S. Fracasso *et al.*, Phys. Rev. C **86**, 044303 (2012)
[42] C. Simenel, Eur. Phys. J. A **48**, 152 (2012)
[43] T. Nakatsukasa *et al.*, Rev. Mod. Phys. **88**, 045004 (2016)
[44] P.A.M. Dirac, Proc. Cambridge Phil. Soc. **26**, 376 (1930)
[45] P. Bonche *et al.*, Phys. Rev. C **13**, 1226 (1976)
[46] J.W. Negele, Rev. Mod. Phys. **54**, 913 (1982)
[47] A. Lazzarini *et al.*, Phys. Rev. C **24**, 309 (1981)
[48] A.S. Umar *et al.*, Phys. Rev. Lett. **56**, 2793 (1986)
[49] T. Otsuka *et al.*, Phys. Rev. Lett. **95**, 232502 (2005)
[50] G. Colò *et al.*, Phys. Lett. B **646**, 227 (2007)
[51] T. Lesinski *et al.*, Phys. Rev. C **76**, 014312 (2007)
[52] M. Bender *et al.*, Phys. Rev. C **80**, 064302 (2009)
[53] V. Hellemans *et al.*, Phys. Rev. C **85**, 014326 (2012)
[54] C.L. Bai *et al.*, Phys. Rev. Lett. **105**, 072501 (2010)
[55] Y. Iwata, J.A. Maruhn, Phys. Rev. C **84**, 014616 (2011)
[56] J. Maruhn *et al.*, Comput. Phys. Commun. **185**, 2195 (2014)
[57] D. Davesne *et al.*, Phys. Rev. C **80**, 024314 (2009)
[58] E. Perlińska *et al.*, Phys. Rev. C **69**, 014316 (2004)
[59] L.C. Vaz *et al.*, Physics Reports **69**, 373 (1981)
[60] E. Chabanat *et al.*, Nucl. Phys. A **635**, 231 (1998)
[61] E. Chabanat *et al.*, Nucl. Phys. A **643**, 441 (1998)
[62] K.A. Brueckner *et al.*, Phys. Rev. **173**, 944 (1968)
[63] C. Simenel, B. Avez, Intl. J. Mod. Phys. E **17**, 31 (2008)
[64] K. Washiyama, D. Lacroix, Phys. Rev. C **78**, 024610 (2008)
[65] C. Simenel, *et al.*, Phys. Rev. C **95**, 031601(R) (2017)
[66] C. Simenel *et al.*, Phys. Rev. C **88**, 064604 (2013)